CellPress

Cell Host & Microbe
Resource

Anticytolytic Screen Identifies Inhibitors of Mycobacterial Virulence Protein Secretion

Jan Rybniker,[1,2] Jeffrey M. Chen,[1] Claudia Sala,[1] Ruben C. Hartkoorn,[1] Anthony Vocat,[1] Andrej Benjak,[1] Stefanie Boy-Röttger,[1] Ming Zhang,[1] Rita Székely,[1] Zoltán Greff,[3] László Őrfi,[3,4] István Szabadkai,[3] János Pató,[3] György Kéri,[3,5] and Stewart T. Cole[1,*]

[1]Global Health Institute, Ecole Polytechnique Fédérale de Lausanne (EPFL), 1015 Lausanne, Switzerland
[2]1st Department of Internal Medicine, University of Cologne, 50937 Cologne, Germany
[3]Vichem Chemie Research Ltd., Herman Otto u. 15, 1022 Budapest, Hungary
[4]Department of Pharmaceutical Chemistry, Semmelweis University, Hőgyes Endre u. 9, 1092 Budapest, Hungary
[5]MTA-SE Pathobiochemistry Research Group, Department of Medical Chemistry, Semmelweis University, 1094 Budapest, Hungary
*Correspondence: stewart.cole@epfl.ch
http://dx.doi.org/10.1016/j.chom.2014.09.008

SUMMARY

Mycobacterium tuberculosis (_Mtb_) requires protein secretion systems like ESX-1 for intracellular survival and virulence. The major virulence determinant and ESX-1 substrate, EsxA, arrests phagosome maturation and lyses cell membranes, resulting in tissue damage and necrosis that promotes pathogen spread. To identify inhibitors of _Mtb_ protein secretion, we developed a fibroblast survival assay exploiting this phenotype and selected molecules that protect host cells from _Mtb_-induced lysis without being bactericidal in vitro. Hit compounds blocked EsxA secretion and promoted phagosome maturation in macrophages, thus reducing bacterial loads. Target identification studies led to the discovery of BTP15, a benzothiophene inhibitor of the histidine kinase MprB that indirectly regulates ESX-1, and BBH7, a benzyloxybenzylidene-hydrazine compound. BBH7 affects _Mtb_ metal-ion homeostasis and revealed zinc stress as an activating signal for EsxA secretion. This screening approach extends the target spectrum of small molecule libraries and will help tackle the mounting problem of antibiotic-resistant mycobacteria.

INTRODUCTION

Tuberculosis (TB), resulting from infection with *Mycobacterium tuberculosis* (*Mtb*), is a serious global health problem accounting for 1.4 million deaths in 2011 (Lechartier et al., 2014). A major reason for the high morbidity and mortality caused by *Mtb* is the long duration of therapy and increasing multidrug resistance. Alternative therapeutic agents are needed to combat drug resistance. By screening compounds in vitro for growth inhibition of *Mtb*, some progress has been made toward clinically implementing bioactive molecules with new mechanisms of action (Lechartier et al., 2014). However, given the high attrition rate of lead compounds in preclinical and clinical development, alternative screening approaches are needed. Traditional *Mtb* whole-cell screens often identify different inhibitors, with the same mechanism of action, of promiscuous targets, a problem that may be solved by more sophisticated phenotypic screens (Lechartier et al., 2014).

Targeting virulence protein secretion can extend the spectrum of existing antibacterial libraries (Feltcher et al., 2010). This radically different approach has been applied to the type III secretion systems (T3SSs) of Gram-negative bacteria (Baron, 2010), which inject virulence determinants into eukaryotic cells. Several structurally unrelated molecules block T3SS protein secretion leading to attenuation and bacterial clearance by the immune system (Izoré et al., 2011).

Mtb has two essential protein export systems that process most of the secretome: the general secretory (Sec) and twin-arginine (Tat) pathways (Braunstein et al., 2003). Five specialized ESX or type VII secretion systems export protein subsets such as virulence determinants (Feltcher et al., 2010). Among these, ESX-1 is a major, well-studied virulence protein secretion apparatus comprising several transmembrane proteins, ATPases, and essential accessory proteins. Additionally, there are several key regulatory proteins that coregulate ESX-1 secretion. Various ESX-1-dependent substrates are essential for host cell invasion, intracellular replication, and inhibition of phagosome maturation (MacGurn and Cox, 2007; Stoop et al., 2012). The best-understood ESX-1 substrate, EsxA, a 6 kDa protein, is capable of lysing cell membranes leading to cytosolic escape and subsequent dissemination of *Mtb* (De Leon et al., 2012). Loss of the ESX-1 genetic locus in *Mycobacterium bovis* accounts for attenuation of the BCG vaccine (Pym et al., 2002).

The regulatory and core proteins of the ESX-1 and housekeeping secretion systems comprise a multitude of interesting and thus far unexploited drug targets (Chen et al., 2010; Feltcher et al., 2010). ESX-1 cannot be targeted by conventional whole-cell screens since it is not essential for bacterial viability in vitro. However, target-based screens have largely failed to provide compounds with reasonable activity on *Mtb* (Lechartier et al., 2014).

CHOM 1136

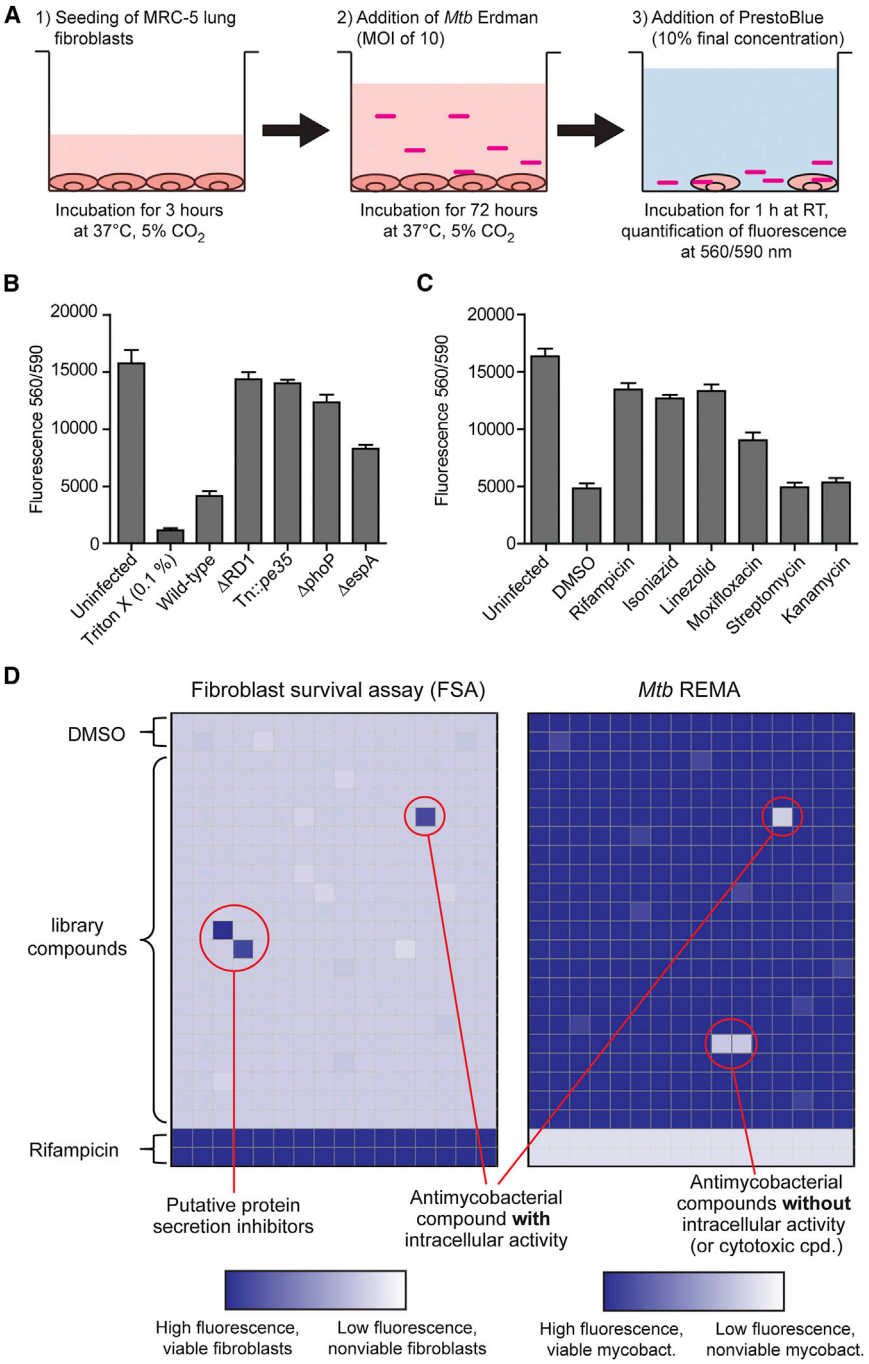

Figure 1. Principle of Fibroblast-Based HTS for Identification of Protein Secretion Inhibitors

(A) Pipetting and incubation scheme of the FSA. For drug screens, compounds were added to empty 384-well plates followed by addition of fibroblasts.

(B) Well-defined ESX-1 mutants are deficient in killing fibroblasts (mean values and ± SD).

(C) Antimycobacterial compounds with intracellular activity protect fibroblasts from *Mtb*-induced cytotoxicity (10 μM, ± SD).

(D) Plate layout for HTS and identification scheme for putative protein secretion inhibitors (see also Figure S1).

RESULTS

Development of a Lung Fibroblast-Based HTS to Identify Protein Secretion Inhibitors

To screen small molecule libraries for inhibitors of mycobacterial protein secretion, we exploited the cytotoxicity of *Mtb* for eukaryotic cells at high multiplicities of infection (MOIs) as described by Hsu et al. and Takii et al. (Hsu et al., 2003; Takii et al., 2002). As proof of principle, MRC-5 lung fibroblasts were infected with the wild-type Erdman strain and well-defined attenuated mutants deficient in ESX-1 secretion followed by quantification of metabolic activity in fibroblasts (Figure 1A). Wild-type *Mtb* was highly cytotoxic, markedly decreasing fluorescence compared to uninfected cells in this fibroblast survival assay (FSA; Figure 1B). The ΔRD1 mutant, lacking core genes in the ESX-1 locus, as well as the Tn::*pe35* mutant that does not produce EsxA due to an upstream transposon insertion, failed to lyse MRC-5 fibroblasts. Furthermore, infection with a deletion mutant of the PhoPR two-component regulatory system or with a Δ*espA* mutant led to significantly less cytotoxicity due to impaired EsxA secretion (Figure 1B) (Chen et al., 2013; Gonzalo-Asensio et al., 2008).

Here we developed a robust, whole-cell-based high-throughput screen (HTS) broad enough to target essentially all structural and regulatory ESX-1 components, yet specific enough to exclude weak compounds. The screen exploited the EsxA-dependent cytolytic activity of *Mtb* and uncovered small molecules that promote survival of *Mtb*-infected human lung fibroblasts by inhibiting ESX-1-dependent protein secretion. The transcriptomic signatures of the most potent hits indicate functions beyond ESX-1 inhibition including cell membrane transport, metal-ion homeostasis, and signal transduction.

We also tested several compounds with known antimycobacterial activity for their ability to protect MRC-5 cells from *Mtb*-induced cell death. As expected, drugs with intracellular activity (rifampicin, isoniazid, linezolid, and moxifloxacin) were highly protective, whereas aminoglycosides (streptomycin and kanamycin), which fail to penetrate MRC-5 cells, were not (Figure 1C). Since the assay endpoint is survival of eukaryotic cells, we tested host-modifying drugs that have been shown to reduce intracellular bacterial load by inhibiting host kinases such as BCR-Abl, Akt, or the secreted mycobacterial kinase PknG (Lechartier et al., 2014). None of these compounds protected fibroblasts

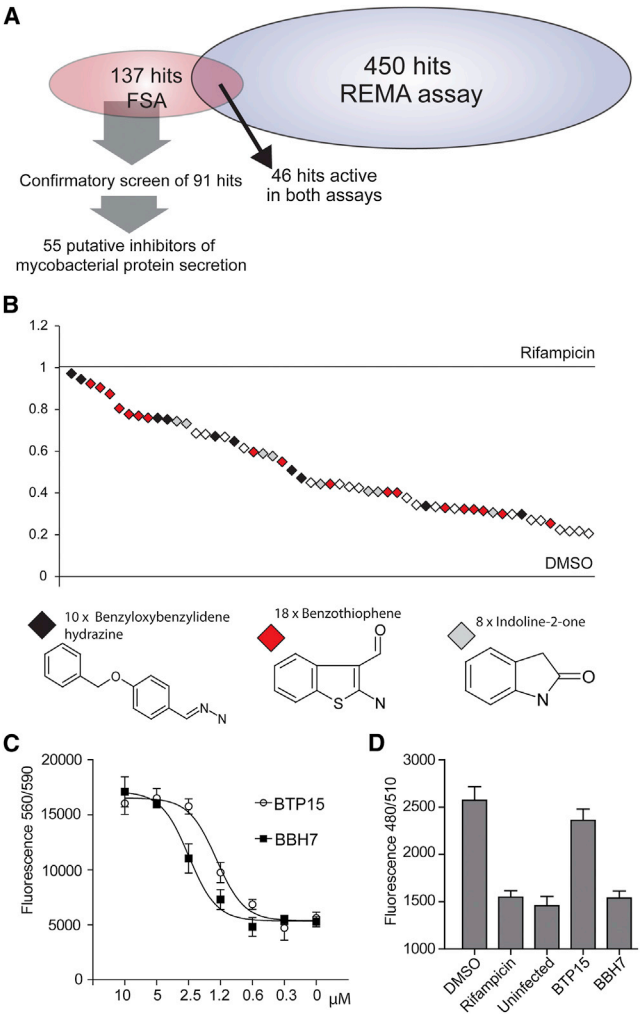

Figure 2. Outcome of Primary and Confirmatory Screens

(A) Hit rate of FSA and REMA in primary and confirmatory screens.

(B) Potency of 55 FSA hit compounds (5 μM) in comparison to rifampicin (5 μg/ml) and DMSO controls. Core structures of three most abundant scaffolds.

(C) BTP15 and BBH7 protect fibroblasts from *Mtb*-induced killing in a dose-dependent manner (± SD).

(D) BTP15 has no influence on GFP expression by *Mtb* indicating that BTP15 is not bactericidal in fibroblasts (5 μM, ± SD), whereas BBH7 reduces the GFP signal comparable to rifampicin-treated fibroblasts (see also Figure S2).

from *Mtb*-induced host cell lysis (Figure S1A available online). Reducing the MOI led to a minor protective effect of some kinase inhibitors (Figure S1A) indicating that their inactivity in the FSA is primarily due to the choice of cell: fibroblasts versus macrophages.

The FSA was adapted for 384-well plates giving a Z′-factor > 0.5 with rifampicin and DMSO as controls (Figure S1B). To distinguish between antivirulence compounds and growth-inhibitory drugs, all compounds were counterscreened against *Mtb* in the resazurin reduction microtiter assay (REMA). A putative protein secretion inhibitor was defined as a hit compound that protected fibroblasts from *Mtb*-induced cell death in the FSA without affecting bacterial growth in the REMA (Figure 1D).

Outcome of the Primary and Confirmatory Screens

A proprietary library of 10,880 synthetic compounds was screened at a concentration of 5 μM leading to the identification of 450 compounds that inhibited mycobacterial growth in the REMA (Figure 2A). A total of 137 compounds were protective in the FSA, and 46 compounds were active in both assays, indicating that only 10% of the REMA hit compounds had intracellular activity and were noncytotoxic for fibroblasts. After a confirmatory screen, 55 of the 91 compounds, which impacted virulence without affecting mycobacterial growth in the primary screen, were validated as true hits (Figure 2A). Cheminformatic analysis identified six clusters and nine singletons. Figure 2B correlates the potency of these hits to the controls and displays the three most abundant core structures. Of note, several analogs of the benzyloxybenzylidene-hydrazines and the benzothiophenes were almost as efficient as rifampicin in protecting fibroblasts from *Mtb*-induced cell death.

For further studies, we selected a benzyloxybenzylidene-hydrazine compound (BBH7) and a benzothiophene compound (BTP15; Figure S2A) with particularly good FSA activity and a favorable cytotoxicity profile. Both compounds protected fibroblasts in a dose-dependent manner (Figure 2C) with an IC_{50} of 2.4 μM for BBH7 and 1.2 μM for BTP15, while no growth inhibition of *Mtb* was observed in vitro at 25 μM concentration (Figure S2B). The MIC_{99} for several other mycobacteria and bacterial pathogens was > 100 μM for both compounds (Figure S2C). Intracellular antimycobacterial activity was determined by quantifying *Mtb* expressing GFP in infected fibroblasts, and here the compounds behaved divergently. BTP15-treated bacteria showed GFP fluorescence comparable to the untreated control, whereas no fluorescence was detected in the BBH7- and rifampicin-treated samples (Figure 2D). These data demonstrate that BTP15 did not affect bacterial viability in the FSA, yet was highly protective for fibroblasts exposed to *Mtb,* whereas BBH7 is a potent inhibitor of intracellular growth.

BBH7 and BTP15 Inhibit Mycobacterial Protein Secretion at Nanomolar Concentrations

The main aim of the FSA is to identify potential inhibitors of ESX-1. We exposed *Mtb* cultures to the compounds, harvested the culture filtrates, and quantified EsxA by immunoblotting. Intriguingly, both compounds showed dose-dependent secretion inhibition of this major virulence protein (Figure 3). We also quantified Ag85 complex proteins, since these are Tat-dependent substrates. At 5 μM, BBH7 fully blocked Ag85 secretion. For BTP15 we observed a different pattern as, at concentrations $\leq$ 10 μM, Ag85 secretion was only slightly affected at best. However, 20 μM BTP15 reduced Ag85 secretion and blocked EsxA secretion fully (Figure 3).

BTP15 Deregulates Genes Controlled by Two-Component Regulatory Systems

RNA-seq experiments with compound-treated *Mtb* provided mechanistic insight from specific transcriptomic signatures. Only 35 genes were differentially regulated when *Mtb* was exposed to 5 μM of BTP15 (Table S1). Surprisingly, all 18 significantly downregulated genes were in the DosR (DevR) regulon (Table S1; Figure 4A). This hypoxia-induced regulon requires the two-component response regulator DosRS, which enables

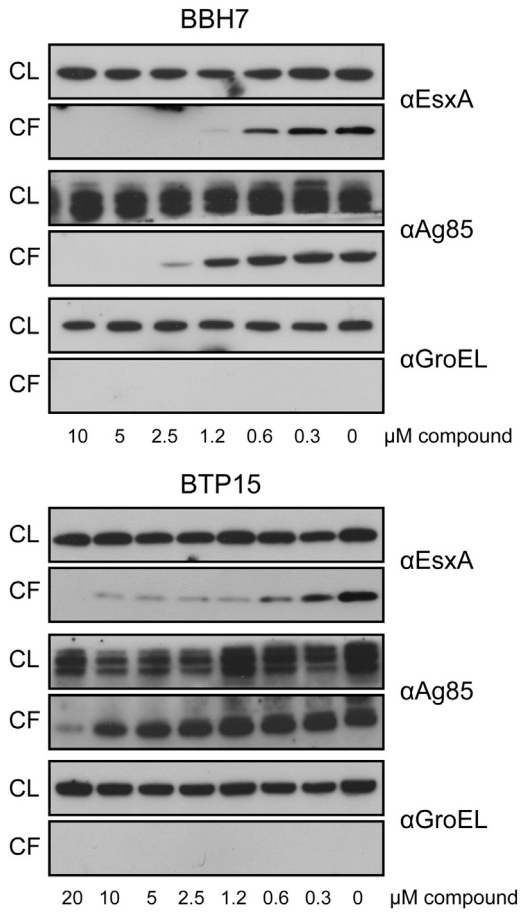

Figure 3. BTP15 and BBH7 Affect EsxA Secretion of *Mtb*
Bacteria were exposed to different concentrations of compound. After 4 days EsxA, Ag85, and GroEL (cell lysis control) were detected by immunoblotting culture filtrate (CF) and cell lysate (CL).

the bacteria to enter a "dormant" nonreplicative state ensuring long-term intracellular survival and latency (Park et al., 2003).

In *Mtb* the response regulators PhoPR and MprAB are known to link the DosR regulon and transcriptional regulation of the ESX-1 secretion system via the distal *espACD* locus (Gonzalo-Asensio et al., 2008; Pang et al., 2007, 2013). Deletion of *mprAB* leads to upregulation of *espA* and reduced EsxA secretion (Pang et al., 2013). In the primary RNA-seq experiment, *espA* was upregulated below the threshold of 2, but on analysis by qRT-PCR, *espA* was among the genes with > 2-fold differential regulation (Figure 4A). Thus, reduced EsxA secretion and the subsequent loss of virulence observed could be caused by deregulation of the *espACD* locus. We then quantified transcription levels of the regulatory genes *dosR*, *phoP*, and *mprA* after exposure to BTP15. Interestingly, *mprA* expression was significantly downregulated after 24 and 48 hr of treatment (Figure 4B). BTP15 (10 μM) also decreased *mprB* transcript levels 3-fold after 48 hr exposure (Figure S3A). Since there is considerable overlap among DosR- and MprA-regulated genes, we compared the BTP15 RNA-seq transcript analysis with published gene expression data on *mprAB* deletion mutants and found that the majority of the 35 deregulated genes (highlighted in Table S1) were also differentially regulated in this mutant under different conditions (He et al., 2006; Pang et al., 2007).

BTP15 Is a Kinase Inhibitor that Inhibits MprB Autophosphorylation In Vitro

Having found that treatment of *Mtb* with BTP15 leads to deregulation of genes controlled by two-component regulatory systems, notably MprAB, we reasoned that the compound might directly affect ATP-dependent signal-transducing histidine kinases. Studying histidine phosphorylation is extremely challenging due to the chemical instability of this posttranscriptional modification (Kee and Muir, 2012). An MprB autophosphorylation assay was established using purified truncated MprB as described (Zahrt et al., 2003). Relatively large amounts of MprB (25 μM) were needed to detect the MprB phosphohistidine (Figure 4C), as is common for histidine kinase phosphorylation assays (Saini and Tyagi, 2005). Nonetheless, we demonstrated dose-dependent inhibition of MprB autophosphorylation by BTP15 (Figure 4D), but could not accurately determine the IC_{50} value due to the large amount of enzyme used. The nonhydrolyzable ATP analog AMP-PNP can be employed to estimate the potency and specificity of histidine kinase inhibitors having high in vitro IC_{50} values (Gilmour et al., 2005). When 10 mM AMP-PNP (34× the in vitro IC_{50} of BTP15) was used, only incomplete reduction of the phosphohistidine signal was seen, whereas 1 mM AMP-PNP had no effect on autophosphorylation (Figure 4D), indicating that BTP15 is a much stronger inhibitor of MprB autophosphorylation than the ATP analog.

BBH7 Has a Pleiotropic Inhibitory Effect on Mycobacterial Protein Secretion

By immunoblotting, BBH7 was found to impact two different protein secretion systems at concentrations $\leq$ 5 μM (Figure 3); we also observed a 50% reduction of total culture filtrate protein when bacteria were exposed to 5 μM BBH7 (data not shown). To appreciate its full impact on protein secretion we characterized and quantified the secretome of treated and untreated bacteria by LC/MS-MS. These data confirmed the inhibitory effect of BBH7 on the ESX-1 secretion system (Table S2). In addition, several substrates of the ESX-5 secretion system such as EsxN, EsxM, PE25, and PPE41 were significantly reduced in abundance upon treatment. Reduced secretion of virulence-associated proteins of unknown export mechanism was uncovered showing that BBH7 affects several independent lines of *Mtb* pathogenicity (Table S2).

BBH7 Deregulates Several Transmembrane ATPases and Alters Mycobacterial Cell-Wall Permeability

Since BBH7 substantially impacted mycobacterial protein secretion, we expected major changes in the *Mtb* transcriptome after treatment. Indeed, RNA-seq experiments revealed 144 differentially regulated genes ($\geq$ 2-fold) upon exposure to BBH7. Of these, 121 were upregulated, and the gene expression signature mirrors changes primarily associated with cell-wall processes and transport (Figures 5A and S4; Table S3). We found positive regulation of the ESX transmembrane ATPase genes *eccCa1/eccCb1* and *eccA5/eccE5* in response to altered ESX-1- and ESX-5-dependent protein secretion. In addition, strong upregulation of the P-type ATPase genes *ctpC* and

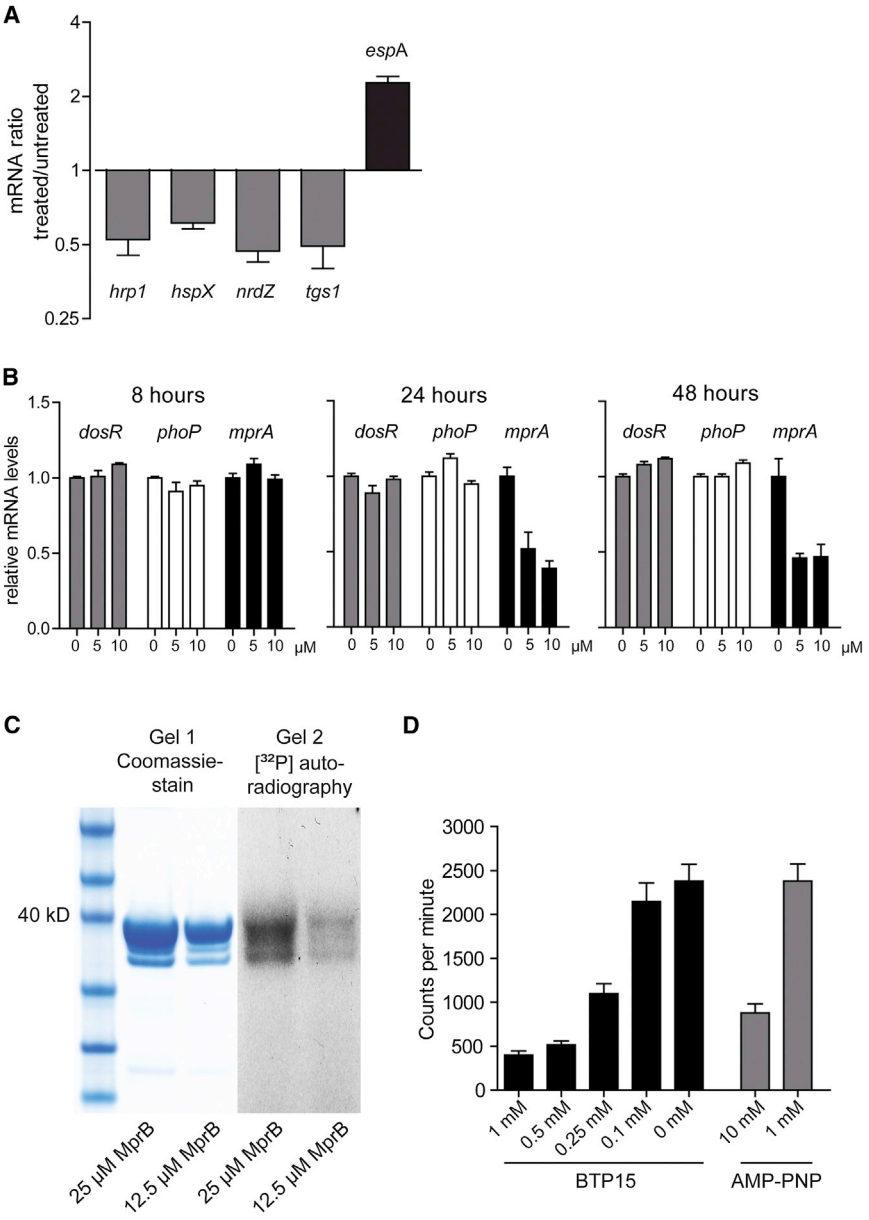

Figure 4. Kinase Inhibitor BTP15 Deregulates Genes of the MprAB Regulon

(A) qRT-PCR of BTP15-treated samples. BTP15 leads to downregulation (> 1.5-fold) of DosR/MprAB-associated genes and upregulation (> 2-fold) of *espA* (± SD).

(B) Transcriptional levels of three two-component regulatory genes followed by qRT-PCR at three different time points after treatment with two different concentrations. BTP15 downregulates *mprA* after 24 and 48 hr of treatment (± SD).

(C) Coomassie blue-stained SDS-PAGE of affinity-purified MprB and autophosphorylation of MprB after incubation with [γ-^{32}P]ATP detected by autoradiography.

(D) 25 µM of MprB was treated with BTP15, and incorporation of ^{32}P was quantified by scintillation counting. BTP15 leads to a dose-dependent inhibition of autophosphorylation. Nonhydrolysable AMP-PNP was used as a control at 1 and 10 mM (± SD) (see also Figure S3; Table S1).

ctpG indicated disturbed cell-membrane/cell-wall transport not only for secreted proteins, but also for ions such as zinc and copper. Several other signs for metal-ion overload were observed: strong upregulation of the metallothionein *mymT*, the multicopper oxidase *mmcO*, the copper-dependent regulator *ricR*, and the RicR-regulated gene *lpqS*, as well as deregulation of the zinc stress-responsive genes *cadI*, *rv1993*, *cysK2*, *esxG*, *and esxH* (Figure 4A; Table S3) (Botella et al., 2011; Serafini et al., 2013). Indirect targets for metal-ion toxicity are Fe-S proteins, explaining the upregulation of the Fe-S cluster biogenesis operon SUF (*rv1462–rv1466*), and DNA damage leading to a LexA-driven transcriptional response (Rowland and Niederweis, 2012).

To investigate whether BBH7 alters mycobacterial outer membrane permeability, which might explain the transcriptomic pattern associated with metal-ion toxicity, we performed ethidium bromide (EtBr) uptake assays after treatment with the compounds of interest. Indeed, BBH7 treatment was found to increase EtBr accumulation and fluorescence, a sign of perturbed membrane permeability (Figure 5B). This was not observed with BTP15. Interestingly, BBH7 concentrations as high as 25 µM had no impact on the activity of first- and second-line TB drugs (Figure S5).

Zinc Stress Augments EsxA Secretion

Having established that BBH7 treatment leads to transcriptional signs of zinc and copper stress, we surmised that intracellular metal-ion stress might be the link to inhibition of mycobacterial protein secretion. Thus, we stressed *Mtb* with physiological concentrations of zinc or copper, as encountered in the phagosome, and determined EsxA secretion levels. Surprisingly, growing cells in media containing elevated levels of $ZnSO_4$ led to a significant and dose-dependent increase of EsxA secretion, whereas Ag85 secretion remained unchanged (Figure 5C). In the presence of 500 µM zinc, a concentration measured in *Mtb*-infected macrophages (Botella et al., 2011), a 6-fold increase in EsxA secretion was observed (Figure 5C, lower panel). Elevated concentrations of copper had no effect on EsxA secretion. These findings indicate that BBH7 does not alter mycobacterial protein secretion by zinc or copper intoxication. Furthermore, we report an environmental signal (elevated zinc levels) that augments EsxA secretion.

Since bacterial transport mechanisms depend on the proton motive force, which is linked to intracellular ATP levels, the intracellular ATP concentration was measured after BBH7 treatment. Unlike treatment with the ATP synthase inhibitor bedaquiline (BDQ), ATP levels were not reduced by BBH7 (Figure 5D). To

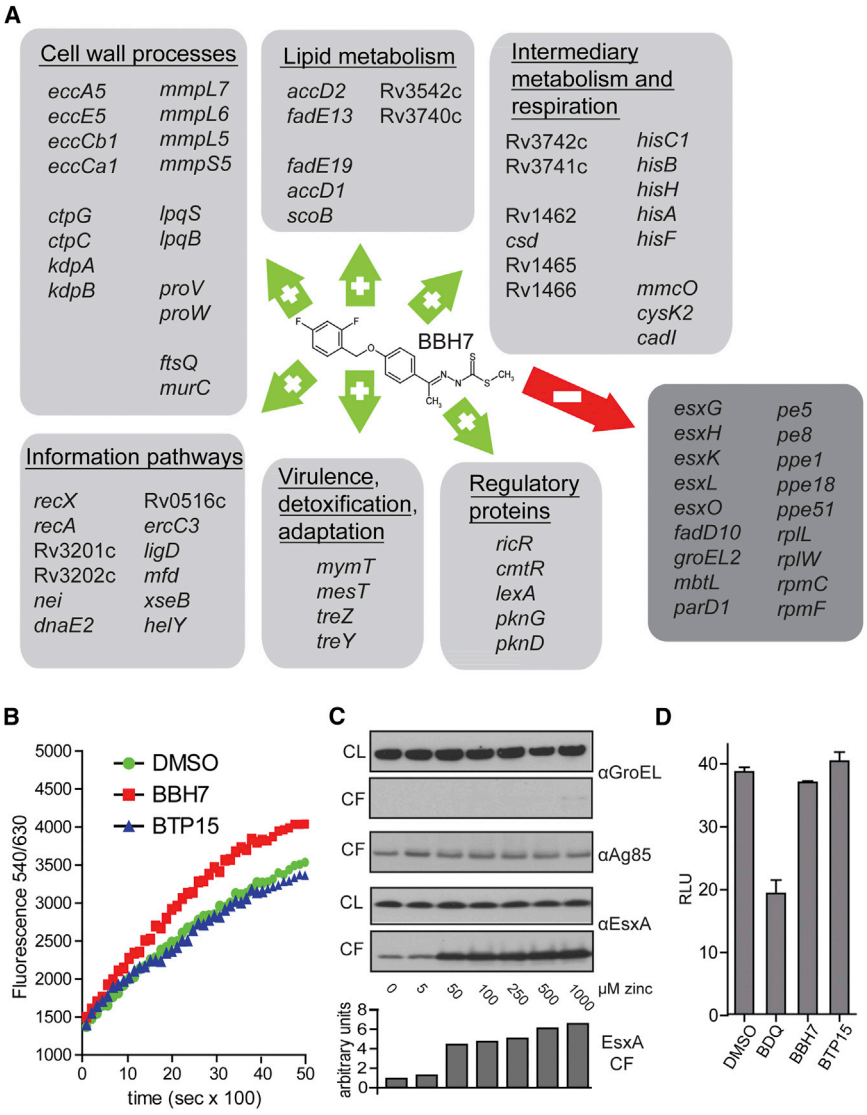

Figure 5. BBH7 Induces Several P-type-ATPases and Alters Outer Membrane Permeability

(A) Selection of up- and downregulated genes upon exposure to BBH7 (5 μM).

(B) BBH7 treatment (10 μM) leads to increased EtBr uptake indicating altered outer membrane permeability. Representative example of three individual experiments.

(C) Addition of zinc strongly induces EsxA secretion in a dose-dependent manner. The Tat substrate Ag85 is not affected by this treatment. Band intensity of EsxA in the CF was quantified in the lower panel (CF, culture filtrate; CL, cell lysate; representative example of three individual experiments).

(D) BBH7 and BTP15 (10 μM) have no impact on ATP levels of *Mtb*; the ATP synthase inhibitor bedaquiline (BDQ, 60 ng/ml) was used as a control. Relative light units (RLUs) were adjusted to OD values (± SD) (see also Figures S4 and S5; Tables S2 and S3).

further distinguish BBH7 from well-known, mycobacterial cell-wall inhibitors, we investigated whether such compounds affect EsxA secretion. Isoniazid and ethambutol, as well as the thiourea compounds ethionamide and thiacetazone, had no effect on EsxA secretion at 0.5 × MIC (Figure S4C). At 5 × MIC, detection of the cytosolic heat-shock protein GroEL in the culture filtrate indicated cell lysis, which was not observed after BBH7 and BTP15 treatment.

Taken together, these results indicate a mechanism of action for BBH7, which alters cell-wall permeability for both export of proteins and import of small molecules, leading to strong upregulation of genes associated with metal-ion overload. However, blockage of EsxA secretion by BBH7 does not seem to be caused by zinc/copper intoxication or ATP depletion.

BBH7 and BTP15 Reduce Intracellular Bacterial Load and Promote Phagolysosomal Fusion in *Mtb*-Infected THP-1 Macrophages

Using GFP-expressing *Mtb* we had shown that BBH7 strongly affects viability of intracellular bacteria in MRC-5 fibroblasts, whereas BTP15 does not (Figure 2D). Since the role of fibroblasts in in vivo infections is not clear, we also investigated the activity of the compounds by infecting activated THP-1 macrophages and quantifying both surviving macrophages and intracellular fluorescent mycobacteria. Treatment with BBH7 and BTP15 protected THP-1 cells from *Mtb*-induced cell death (Figure 6A) and greatly reduced the intracellular bacterial load (Figures 6B and 6C). Since the ESX-1 secretion system plays a decisive role in the arrest of phagosome maturation in *Mtb*-infected macrophages (MacGurn and Cox, 2007), we investigated whether BBH7 and BTP15 can reverse this phenotype. Activated THP-1 macrophages were infected at an MOI of 0.5 with *Mtb* expressing GFP and treated for 7 days. Subsequently, acidic compartments were stained with Lysotracker Red, and colocalization of the dye with fluorescent mycobacteria was quantified by confocal microscopy. Treated bacteria were found in acidic compartments at significantly higher levels than untreated bacteria (Figures 6D and 6E) indicating that reduction of intracellular bacterial load in macrophages is primarily achieved through inhibition of *Mtb*-induced phagosome maturation arrest.

DISCUSSION

In this investigation, we developed and validated a phenotypic drug screen based on ESX-1 secretion-dependent cytotoxicity of *Mtb*. A HTS of > 10,000 small molecules identified two series of compounds that significantly reduced secretion of EsxA at nanomolar concentrations without affecting mycobacterial growth in vitro, the benzothiophenes and benzyloxybenzylidene-hydrazines. In addition, less potent hit compounds derived

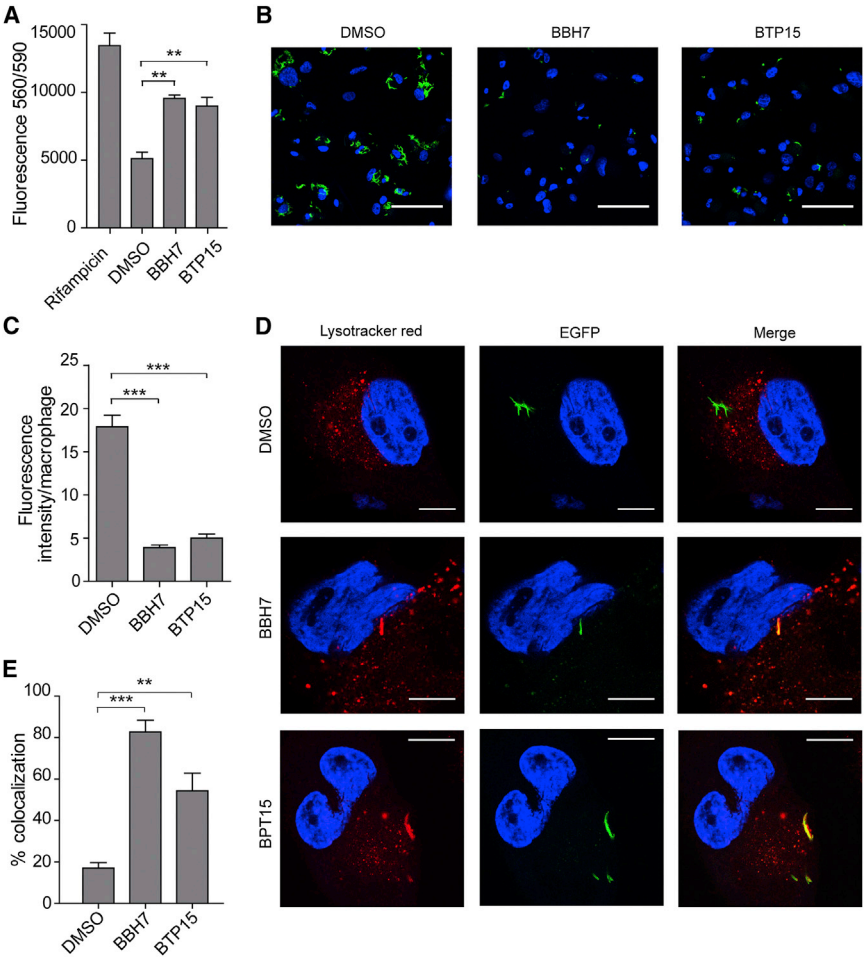

Figure 6. BTP15 and BBH7 Promote Phagolysosomal Fusion and Reduce Bacterial Load in Activated THP-1 Macrophages

(A) Survival of activated THP-1 macrophages was quantified as performed with MRC-5 lung fibroblasts. Both compounds (10 μM) protect the cells from *Mtb*-induced cytotoxicity.

(B and C) *Mtb*-GFP was quantified inside activated THP-1 cells after treatment with BBH7 and BTP15 (10 μM) as described in Experimental Procedures. Both compounds significantly reduce the intracellular bacterial load. For BTP15, this contrasts with treatment of infected fibroblasts where intracellular replication is not affected (Figure 2D). Scale bar, 100 μm.

(D and E) Confocal microscopy of infected THP-1 macrophages after treatment with two compounds (10 μM) or vehicle (DMSO). After 7 days, acidic compartments were stained with Lysotracker Red, and colocalization of *Mtb*-GFP with these compartments was quantified (scale bar, 20 μm). Both compounds promote phagolysosomal fusion to higher levels than DMSO-treated bacteria. ***$p \leq 0.001$, **$p \leq 0.01$ (± SD).

from the indoline-2-one core structure as well as several other compounds impacted ESX-1 function (data not shown). This indicates that by selecting for hits that abrogate cytotoxicity of *Mtb*, the chance of finding inhibitors of ESX-1-dependent protein secretion is relatively high. The reason for this may lie in the nature of the screen itself; *Mtb*-induced host cell lysis at high MOI is almost exclusively associated with secretion of EsxA. Screening deep transposon libraries for mutants with impaired cytolytic activity primarily detected insertions in genes required for EsxA secretion, thus highlighting the importance of this virulence determinant (Gao et al., 2004; Hsu et al., 2003). Another key factor for selectivity of the bioassay is our choice of lung fibroblasts for the quantification of *Mtb*-induced cell death. These nonprofessional phagocytes fail to detect host-modifying agents that reduce the intracellular burden of *Mtb* in macrophages (Lechartier et al., 2014). This feature may be beneficial for target identification of these antivirulence drugs.

The benzothiophene BTP15 is a kinase inhibitor that affects EsxA secretion most likely by deregulating the *espACD* operon. Several transcriptional regulators control ESX-1-dependent secretion by binding to this operon that is not part of the ESX-1 region, but nonetheless encodes EsxA cosecreted proteins (Blasco et al., 2012; Gonzalo-Asensio et al., 2008; Pang et al., 2013). An *mprAB* mutant displayed upregulation of *espA* and greatly reduced EsxA secretion (Pang et al., 2013). Furthermore, MprA coregulates several DosR-regulated genes and SigE (Pang et al., 2007). BTP15 treatment deregulates a similar set of genes and inhibits MprB autophosphorylation in vitro. Thus, the two-component regulatory system MprAB is the probable BTP15 target. MprAB is clearly associated with virulence since the corresponding mutants show impaired survival in vivo, particularly during the chronic stage of infection (Zahrt and Deretic, 2001). Macrophages infected with a Δ*mprAB* strain elicit significantly lower levels of tumor necrosis factor alpha and interleukin 1β similar to *Mtb* strains deleted for *espACD* or the ESX-1 region (Pang et al., 2013). MprAB also seems to regulate the ESX-1 region itself since the *mprAB* mutant fails to secrete EspB, a protein that is not influenced by the *espACD* operon (Chen et al., 2013; Pang et al., 2013). We also found inhibition of EspB secretion upon BTP15 treatment (Figure S3B), accompanied by greater attenuation than seen with a Δ*espA* mutant in the FSA. However, in contrast to BTP15-treated macrophages, which show reduced intracellular bacterial load, loss of *mprAB* does not reduce the number of intracellular bacteria in activated macrophages (Zahrt and Deretic, 2001). Low expression levels of *dosR*, *phoP*, and *mprA* were revealed by qRT-PCR experiments, although subtle transcriptional changes during drug treatment may not have been detected. Many of the ESX-1 regulatory genes are induced during intracellular infection, thus BTP15 may have an extended impact on virulence gene expression inside macrophages and fibroblasts, explaining the discrepancy between the intracellular behavior of the Δ*mprAB* mutant and BTP15-treated bacteria.

Bacterial histidine sensor kinases and two-component regulatory systems are indeed interesting drug targets. Potent inhibitors with good in vivo activity have been generated for Gram-negative pathogens (Rasko et al., 2008). Deletions of these

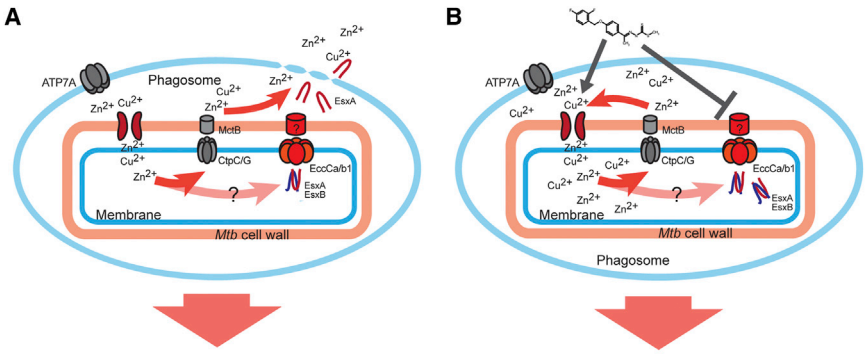

Figure 7. Model for Zinc-Induced EsxA Secretion and Implications for BBH7 Function

(A) After phagocytozing *Mtb* macrophages recruit heavy metal-transporting ATPases like ATP7A to the phagosomal membrane leading to intraphagosomal accumulation of toxic amounts of copper and zinc. This triggers a mycobacterial response involving upregulation of P-type ATPases (CtpC/CtpG) and metal-chelating proteins to clear intracellular copper and zinc. In addition, elevated zinc concentrations induce secretion of EsxA leading to subsequent phagosomal damage and ion efflux thus providing a second line of defense against host-driven heavy metal intoxication.

(B) Treatment with BBH7 alters mycobacterial outer membrane permeability leading to transcriptional signs of copper and zinc stress. CtpC and CtpG will promote heavy metal efflux into the phagosomal vacuole. In parallel, the ESX-1-translocating ATPases EccCa1 and EccCb1 are upregulated; however, EsxA secretion is blocked, probably leading to phagosomal integrity, further heavy metal accumulation in the phagosome, and poisoning of *Mtb*.

regulatory genes often cause severe attenuation as illustrated impressively by the *Mtb* Δ*phoPR* mutant, which is currently being developed as a live TB vaccine (Gonzalo-Asensio et al., 2008). Histidine kinase domains are structurally distinct from eukaryotic serine, threonine, and tyrosine kinases, and this may enable kinase inhibitors with selective antibacterial activity to be developed (Kee and Muir, 2012). However, unlike serine, threonine, and tyrosine kinases, where a plethora of in vitro and in vivo tools are available, histidine kinase research is handicapped by a lack of biochemical tools, largely due to the chemical instability of this posttranslational modification (Kee and Muir, 2012). Nevertheless, with the FSA we provide a validated assay for targeting membrane-bound kinases and other ESX-1 regulatory proteins with small molecules.

While there is considerable knowledge of the proteins involved in transmembrane export of substrates, nothing is known of the fate of proteins once translocated to the periplasm, nor of the mechanism for export through the mycomembrane. Again, putative pore and channel proteins involved in these processes may be interesting drug targets due to their extracytoplasmic location, which may facilitate drug accessibility. This notion is supported by the discovery of a broad-spectrum inhibitor of three unrelated secretion systems in Gram-negative pathogens that is believed to target outer-membrane pore proteins shared by several translocation systems (Felise et al., 2008). With BBH7 we identified a pleiotropic inhibitor of mycobacterial protein secretion. However, the gene expression signature following exposure to BBH7, with strong upregulation of several P-type ATPases as well as altered EtBr uptake in treated bacteria, suggests disturbed export not only for proteins, but also for smaller molecules. This makes a common pore structure exclusively dedicated to protein transport through the cell envelope an unlikely target of BBH7. Rather, it is conceivable that this compound has a more general impact on processes involved in cell-wall biogenesis.

Another possible mechanism of action for BBH7 is depletion of the ATP source for the membrane-bound transport ATPases that is linked to the proton-motive force. Although some protonophores also inhibit bacterial protein translocation, we provide several independent data sets that functionally separate BBH7. First, protonophores are known to deplete the intracellular ATP pool of *Mtb* rapidly (Boshoff et al., 2004), which was not the case for treatment with BBH7. Second, the transcriptional signature of protonophore compounds, with strong upregulation of the *cyd*-operon and genes of the respiratory chain (Boshoff et al., 2004), is distinct from the BBH7 response. Third, unlike BBH7, the nonselective protonophores are highly cytotoxic for *Mtb* (Brown and Parish, 2008) as well as for eukaryotic cells.

There are distinct signs of zinc and copper stress in bacteria exposed to BBH7. Intraphagosomal zinc/copper accumulation as a means for host defense has emerged as an exciting field in mycobacterial research (Botella et al., 2011; Rowland and Niederweis, 2012). In this context, our finding of zinc-enhanced secretion of EsxA might represent a mycobacterial defense mechanism to counteract heavy metal toxicity. Until now, the environmental signals inducing secretion of EsxA have been poorly understood. We propose a model where, after phagocytosis, the cation exporters CtpC and CtpG are upregulated to rapidly relieve cytosolic zinc stress (Figure 7A). However, the phagosome is a closed environment, so the initial upregulation of P-type ATPases will reduce zinc levels in the bacterial cytosol, but not in the phagosome. More sustained alleviation of metal-ion stress may be via EsxA-mediated lysis of the phagosomal membrane (Figure 7A). In fact, EsxA-dependent leakage of potassium ions and efflux of charged fluorophores from phagosomal membranes was recently reported (De Leon et al., 2012). Pore-forming toxin-dependent ion efflux from the phagosome or the host cell membrane is a hallmark of most intracellular bacterial pathogens (Gonzalez et al., 2008).

This model also implies a dual and probably synergistic effect of BBH7 on mycobacterial virulence. BBH7 increases outer membrane permeability and leads to heavy metal stress. The bacterium responds by upregulating the EsxA-translocating ATPases EccCb1 and EccCa1; however, EsxA secretion is blocked by BBH7, which leaves the phagosomal membrane intact and possibly leads to further accumulation of toxic substances in the phagosome (Figure 7B). This mechanism may explain the high rate of phagocytosed bacteria colocalizing

with lysosomes and the potent intracellular growth inhibition we observed in BBH7-treated macrophages and fibroblasts. Of note, there is evidence that the ESX-3 secretion system is involved in zinc homeostasis of *Mtb* (Serafini et al., 2013). Thus, interference with ESX-3 activity by BBH7 may cause the zinc stress observed.

The molecules identified in this work would have escaped detection by conventional whole-cell screens. By selecting for a specific phenotype strongly associated with mycobacterial virulence, the hit spectrum of a given library can be extended as demonstrated here. We also show that molecules protecting eukaryotic cells from *Mtb*-induced cytotoxicity may affect mycobacterial virulence beyond EsxA secretion (dormancy, small molecule influx). The data indicate that antivirulence drugs are capable of reducing the intracellular bacterial load by inducing phagosomal processing in professional phagocytes at levels similar to first-line drugs (Ramachandra et al., 2005).

Our assay format provides both a rapid readout and information about the bactericidality, antivirulence effect, cytotoxicity, and intracellular activity of the hits. Screening novel compound libraries or rescreening existing collections using the FSA may identify additional hits, with mechanisms of action appropriate for lead optimization. Furthermore, compounds from other intracellular screens showing a discrepancy between intracellular IC_{50} and MIC in broth should be tested for inhibition of EsxA secretion, which may facilitate identification of their targets. Finally, our robust screening strategy based on inhibition of pathogen-driven host cell toxicity could also be adopted for antivirulence drug screens targeting toxin-secreting bacteria such as *Clostridium difficile* where alternative treatment approaches are urgently needed.

EXPERIMENTAL PROCEDURES

Bacterial Culture Conditions and Eukaryotic Cell Lines

Full description of experimental procedures and reagents used can be found in Supplemental Information. Mycobacterial strains were routinely grown in Middlebrook 7H9 broth (supplemented with 0.2% glycerol, 10% ADC, and 0.05% Tween 80) or in Sauton's medium for culture filtrate analysis. ESX-1 mutants used for proof of principle studies were H37Rv-ΔRD1, *Mtb* Erdman Tn::*pe35*, *Mtb* Erdman-Δ*espA* (Chen et al., 2013), and *Mtb*-MT103 Δ*phoP* (Gonzalo-Asensio et al., 2008). MRC-5 human lung fibroblasts from the Coriell Institute for Medical Research were grown in MEM medium supplemented with 10% heat-inactivated fetal bovine serum (FBS), 1% nonessential amino acids, and 1 mM sodium pyruvate. THP-1 macrophages were grown in RPMI medium supplemented with 10% FBS. Both cell lines were grown at 37°C with 5% CO_2.

HTS

Library compounds were preplated into CellBIND 384-well microplates (Corning Life Sciences) at a concentration of 50 μM in 5 μl of 5% DMSO. MRC-5 cells grown to late log phase were harvested and seeded at 4,000 cells/well in a volume of 35 μl using an automated microplate dispenser (Multidrop Combi, Thermo Scientific). Cells were allowed to adhere for 3 hr before washed, and midlogarithmic-phase *Mtb* Erdman cells were added to the assay plates at an MOI of 10 in 10 μl of MEM medium. Plates were sealed and incubated at 37°C under 5% CO_2. Rifampicin (5 μg/ml) was used as a control (see Figure 1) for assay plate layout. After 72 hr, plates were left at room temperature (RT) for 1 hr, and 5 μl of PrestoBlue Cell Viability Reagent (Life Technologies) was added. After 1 hr at RT, fluorescence was measured in a Tecan Infinite M200 plate reader (excitation 570 nm, emission 590 nm; fluorescence generated by the bacteria was negligible). REMA assays were performed in 7H9 broth using a starting OD of 0.0001, a 7-day incubation period, and a final volume of 10% resazurin (0.025% w/v). Z′-factor determinations were as described in Supplemental Information. Replicates were considered as hits if their values were superior to the mean of the negative control values plus three standard deviations. The final score was the mean value of the replicates.

Immunoblots and Secretome Analysis

Protein preparation and immunoblots were performed as described recently (Chen et al., 2013). In brief, 30 ml of bacteria grown to midlogarithmic phase (OD_{600} of 0.6–0.7) in Sauton's medium supplemented with 0.05% Tween 80 were centrifuged and resuspended in Sauton's medium without Tween. Compounds were added at concentrations as indicated, and cells were grown further at 37°C with shaking for 4 days. Cultures were harvested by centrifugation to obtain culture filtrates and cell pellets. Culture filtrates were concentrated 100-fold in 5 kDa cutoff Vivaspin columns (Sartorius). Cell lysates were prepared by bead beating bacterial pellets in lysis buffer with 100 μm glass beads.

For immunoblotting, 5 μg of protein was resolved by SDS-PAGE and transferred to nitrocellulose membranes. Membranes were blocked with TBS buffer (3% milk powder) and incubated overnight with the desired primary antibody diluted in TNT buffer supplemented with 1% BSA fraction V. Membranes were washed with TNT, incubated with the appropriate secondary antibody in TNT-BSA, washed again with TNT, and developed. GroEL2 was used as lysis control for culture filtrates and loading control for cell lysates.

Protein preparation for secretome analysis, dimethyl labeling, and mass spectrometry were performed as described in Supplemental Experimental Procedures.

RNA Extraction, qRT-PCR, and RNA-seq

For transcriptomics, bacteria were grown under the same conditions as for protein secretion assays. Drug exposure was 8 hr at 5 μM for RNA-seq experiments and confirmatory qRT-PCR. RNA was extracted with TRIzol (Invitrogen) and treated with DNase I (Roche) prior to library preparation or generation of the cDNA template. cDNA was synthesized using the RevertAid First Strand cDNA Synthesis Kit (Fermentas) using random hexamer primers. cDNA corresponding to 10 ng of input RNA was used in each RT-PCR reaction supplemented with specific primer pairs (200 nM each) listed in Supplemental Information and SYBR-Green Master Mix (Applied Biosystems). Quantitative RT-PCR reactions were performed with the 7900HT Fast Real-Time PCR System (Applied Biosystems) as follows: 50°C for 2 min, 95°C for 10 min, then 40 cycles of 95°C for 15 s and 60°C for 60 s. Melt curve analysis confirmed specific amplification for each primer pair.

For the RNA-seq library preparation, 100 ng of total RNA was used in the TruSeq Stranded mRNA LT Kit, according to the instructions provided by Illumina. An aliquot was analyzed on Qubit (Life Technologies) and Fragment Analyzer (Advanced Analytical) prior to sequencing on an Illumina HiSeq using the TruSeq SR Cluster Generation Kit v3 and TruSeq SBS Kit v3. Data were processed with the Illumina Pipeline Software v1.82. RNA-seq data were deposited in the Gene Expression Omnibus (GEO) server at the National Center for Biotechnology Information (NCBI).

Quantification of Intracellular ATP Levels and EtBr Uptake Assays

Bacteria were grown for 24 hr with test compounds, and the BacTiter-Glo viability reagent (Promega) was used to quantify ATP levels as per the manufacturer's recommendations. For EtBr uptake assays, bacteria were washed with PBS containing 0.05% Tween 80, OD_{600} was adjusted to 0.4, and 100 μl were pipetted into black 96-well plates. EtBr was added (4 μM final concentration), and fluorescence was read every 2 min at 545/600 nm.

Fluorescence Microscopy

THP-1 macrophages were activated on round 9 mm coverslips in 24-well plates (10^5 cells/well) with 100 nM of phorbol-12-myristate-13-acetate for 72 hr. To quantify intracellular *Mtb* Erdman-GFP, macrophages were infected at an MOI of 2 for 12 hr. Cells were washed to remove unphagocytosed bacteria, and fresh medium containing compounds or DMSO was added. After incubation for 4 days, cells were washed, fixed with 4% paraformaldehyde/PBS, and stained with Dapi-Fluoromount-G (SouthernBiotech). Images were acquired on a Zeiss LSM 700 using ZEN imaging software and Fiji processing software. At least 40 fields of three separate monolayers were collected for image processing and statistical analysis. For intracellular localization studies,

cells were prepared as described above and infected at an MOI of 0.5. After 12 hr, extracellular bacteria were removed by washing with PBS, and fresh medium containing compounds or DMSO was added. Incubation continued for a total of 7 days with replacement of media plus compounds after 3 days. Fresh medium containing 50 nM Lysotracker Red (Life Technologies) was added for 2 hr. Cells were washed and fixed as described above. Colocalization rates of GFP-fluorescing phagosomes and Lysotracker Red were determined by analyzing > 100 phagosomes from at least three separate monolayers.

Protein Purification and Kinase Inhibitor Assay

Proteins were purified as described (Rybniker et al., 2014). For autophosphorylation assays, MprB lacking its N-terminal transmembrane domain was incubated with [γ-^{32}P]ATP (10 mCi/ml, 3,000 Ci/mmol) in 50 mM Tris-HCl (pH 7.5), 50 mM KCl, and 20 mM $MnCl_2$ for 1 hr. Reactions were stopped by heating in SDS loading buffer for 5 min at 80°C followed by sample separation using SDS-PAGE. Gels were either stained with Coomassie brilliant blue or dried for 2 hr at 60°C in a Model 583 Gel Dryer (Bio-Rad) followed by exposure to X-ray film overnight or counting of ^{32}P incorporation into band equivalents using an LS6500 Scintillation Counter (Beckman Coulter). For kinase inhibitor assays, compounds were preincubated with MprB for 3 hr prior to addition of [γ-^{32}P]ATP.

Statistical Analyses

Unpaired Student's t tests were used throughout.

ACCESSION NUMBERS

The NCBI Gene Expression Omnibus accession number for the RNAseq data reported in this paper is GSE58314.

SUPPLEMENTAL INFORMATION

Supplemental Information includes five figures, three tables, and Supplemental Experimental Procedures and can be found with this article online at http://dx.doi.org/10.1016/j.chom.2014.09.008.

AUTHOR CONTRIBUTIONS

J.R. and S.T.C. designed the study. J.R., J.M.C., C.S., R.C.H., A.V., S.B.-R., M.Z., and R.S. performed biological experiments and analyzed the data. A.B. performed bioinformatics. Z.G., L.Ő., I.S., J.P., and G.K. designed and synthesized compounds and analyzed chemistry results. J.R. and S.T.C. wrote the paper with input and approval from all authors.

ACKNOWLEDGMENTS

We thank our EPFL colleagues M. Chambon, D. Banfi, and N. Ballanfat for help with assay development; D. Chiappe and R. Hamelin for mass spectrometry; T. Laroche and R. Guillet for confocal microscopy; N. Dhar for providing strains; and S. Georgeon and O. Hantschel for advice on kinase assays. This work was supported in part by grants from Vichem and the Swiss National Science Foundation (grant number 31003A_140778). J.R. was supported by the German Federal Ministry of Research and Education (BMBF grant 01KI1017) and R.S. by a European Commission Marie Curie Fellowship (PIEF-GA-2012-327219). G.K. is the CEO/CSO and founder of Vichem Chemie Research Ltd.; L.Ő. is the cofounder, COO, and VP of Chemistry; G.K., L.Ő., Z.G., I.S., and J.P. are Vichem employees. J.R., G.K., L.Ő., Z.G., I.S., J.P., and S.T.C. are named inventors on a patent pertaining to this work.

Received: June 6, 2014
Revised: August 20, 2014
Accepted: September 17, 2014
Published: October 8, 2014

REFERENCES

Baron, C. (2010). Antivirulence drugs to target bacterial secretion systems. Curr. Opin. Microbiol. *13*, 100–105.

Blasco, B., Chen, J.M., Hartkoorn, R., Sala, C., Uplekar, S., Rougemont, J., Pojer, F., and Cole, S.T. (2012). Virulence regulator EspR of *Mycobacterium tuberculosis* is a nucleoid-associated protein. PLoS Pathog. *8*, e1002621.

Boshoff, H.I., Myers, T.G., Copp, B.R., McNeil, M.R., Wilson, M.A., and Barry, C.E., III. (2004). The transcriptional responses of *Mycobacterium tuberculosis* to inhibitors of metabolism: novel insights into drug mechanisms of action. J. Biol. Chem. *279*, 40174–40184.

Botella, H., Peyron, P., Levillain, F., Poincloux, R., Poquet, Y., Brandli, I., Wang, C., Tailleux, L., Tilleul, S., Charrière, G.M., et al. (2011). Mycobacterial p(1)-type ATPases mediate resistance to zinc poisoning in human macrophages. Cell Host Microbe *10*, 248–259.

Braunstein, M., Espinosa, B.J., Chan, J., Belisle, J.T., and Jacobs, W.R., Jr. (2003). SecA2 functions in the secretion of superoxide dismutase A and in the virulence of *Mycobacterium tuberculosis*. Mol. Microbiol. *48*, 453–464.

Brown, A.C., and Parish, T. (2008). Dxr is essential in *Mycobacterium tuberculosis* and fosmidomycin resistance is due to a lack of uptake. BMC Microbiol. *8*, 78.

Chen, J.M., Pojer, F., Blasco, B., and Cole, S.T. (2010). Towards anti-virulence drugs targeting ESX-1 mediated pathogenesis of *Mycobacterium tuberculosis*. Drug Discov. Today Dis. Mech. *7*, e25–e31.

Chen, J.M., Zhang, M., Rybniker, J., Boy-Röttger, S., Dhar, N., Pojer, F., and Cole, S.T. (2013). *Mycobacterium tuberculosis* EspB binds phospholipids and mediates EsxA-independent virulence. Mol. Microbiol. *89*, 1154–1166.

De Leon, J., Jiang, G., Ma, Y., Rubin, E., Fortune, S., and Sun, J. (2012). *Mycobacterium tuberculosis* ESAT-6 exhibits a unique membrane-interacting activity that is not found in its ortholog from non-pathogenic *Mycobacterium smegmatis*. J. Biol. Chem. *287*, 44184–44191.

Felise, H.B., Nguyen, H.V., Pfuetzner, R.A., Barry, K.C., Jackson, S.R., Blanc, M.P., Bronstein, P.A., Kline, T., and Miller, S.I. (2008). An inhibitor of gram-negative bacterial virulence protein secretion. Cell Host Microbe *4*, 325–336.

Feltcher, M.E., Sullivan, J.T., and Braunstein, M. (2010). Protein export systems of *Mycobacterium tuberculosis*: novel targets for drug development? Future Microbiol. *5*, 1581–1597.

Gao, L.Y., Guo, S., McLaughlin, B., Morisaki, H., Engel, J.N., and Brown, E.J. (2004). A mycobacterial virulence gene cluster extending RD1 is required for cytolysis, bacterial spreading and ESAT-6 secretion. Mol. Microbiol. *53*, 1677–1693.

Gilmour, R., Foster, J.E., Sheng, Q., McClain, J.R., Riley, A., Sun, P.M., Ng, W.L., Yan, D., Nicas, T.I., Henry, K., and Winkler, M.E. (2005). New class of competitive inhibitor of bacterial histidine kinases. J. Bacteriol. *187*, 8196–8200.

Gonzalez, M.R., Bischofberger, M., Pernot, L., van der Goot, F.G., and Frêche, B. (2008). Bacterial pore-forming toxins: the (w)hole story? Cell. Mol. Life Sci. *65*, 493–507.

Gonzalo-Asensio, J., Mostowy, S., Harders-Westerveen, J., Huygen, K., Hernández-Pando, R., Thole, J., Behr, M., Gicquel, B., and Martín, C. (2008). PhoP: a missing piece in the intricate puzzle of *Mycobacterium tuberculosis* virulence. PLoS ONE *3*, e3496.

He, H., Hovey, R., Kane, J., Singh, V., and Zahrt, T.C. (2006). MprAB is a stress-responsive two-component system that directly regulates expression of sigma factors SigB and SigE in *Mycobacterium tuberculosis*. J. Bacteriol. *188*, 2134–2143.

Hsu, T., Hingley-Wilson, S.M., Chen, B., Chen, M., Dai, A.Z., Morin, P.M., Marks, C.B., Padiyar, J., Goulding, C., Gingery, M., et al. (2003). The primary mechanism of attenuation of bacillus Calmette-Guerin is a loss of secreted lytic function required for invasion of lung interstitial tissue. Proc. Natl. Acad. Sci. USA *100*, 12420–12425.

Izoré, T., Job, V., and Dessen, A. (2011). Biogenesis, regulation, and targeting of the type III secretion system. Structure *19*, 603–612.

Kee, J.M., and Muir, T.W. (2012). Chasing phosphohistidine, an elusive sibling in the phosphoamino acid family. ACS Chem. Biol. *7*, 44–51.

Lechartier, B., Rybniker, J., Zumla, A., and Cole, S.T. (2014). Tuberculosis drug discovery in the post-post-genomic era. EMBO Mol. Med. *6*, 158–168.

MacGurn, J.A., and Cox, J.S. (2007). A genetic screen for *Mycobacterium tuberculosis* mutants defective for phagosome maturation arrest identifies components of the ESX-1 secretion system. Infect. Immun. *75*, 2668–2678.

Pang, X., Vu, P., Byrd, T.F., Ghanny, S., Soteropoulos, P., Mukamolova, G.V., Wu, S., Samten, B., and Howard, S.T. (2007). Evidence for complex interactions of stress-associated regulons in an mprAB deletion mutant of *Mycobacterium tuberculosis*. Microbiology *153*, 1229–1242.

Pang, X., Samten, B., Cao, G., Wang, X., Tvinnereim, A.R., Chen, X.L., and Howard, S.T. (2013). MprAB regulates the espA operon in *Mycobacterium tuberculosis* and modulates ESX-1 function and host cytokine response. J. Bacteriol. *195*, 66–75.

Park, H.D., Guinn, K.M., Harrell, M.I., Liao, R., Voskuil, M.I., Tompa, M., Schoolnik, G.K., and Sherman, D.R. (2003). Rv3133c/dosR is a transcription factor that mediates the hypoxic response of *Mycobacterium tuberculosis*. Mol. Microbiol. *48*, 833–843.

Pym, A.S., Brodin, P., Brosch, R., Huerre, M., and Cole, S.T. (2002). Loss of RD1 contributed to the attenuation of the live tuberculosis vaccines *Mycobacterium bovis* BCG and *Mycobacterium microti*. Mol. Microbiol. *46*, 709–717.

Ramachandra, L., Smialek, J.L., Shank, S.S., Convery, M., Boom, W.H., and Harding, C.V. (2005). Phagosomal processing of *Mycobacterium tuberculosis* antigen 85B is modulated independently of mycobacterial viability and phagosome maturation. Infect. Immun. *73*, 1097–1105.

Rasko, D.A., Moreira, C.G., Li, R., Reading, N.C., Ritchie, J.M., Waldor, M.K., Williams, N., Taussig, R., Wei, S., Roth, M., et al. (2008). Targeting QseC signaling and virulence for antibiotic development. Science *321*, 1078–1080.

Rowland, J.L., and Niederweis, M. (2012). Resistance mechanisms of *Mycobacterium tuberculosis* against phagosomal copper overload. Tuberculosis (Edinb.) *92*, 202–210.

Rybniker, J., Pojer, F., Marienhagen, J., Kolly, G.S., Chen, J.M., van Gumpel, E., Hartmann, P., and Cole, S.T. (2014). The cysteine desulfurase IscS of *Mycobacterium tuberculosis* is involved in iron-sulfur cluster biogenesis and oxidative stress defence. Biochem. J. *459*, 467–478.

Saini, D.K., and Tyagi, J.S. (2005). High-throughput microplate phosphorylation assays based on DevR-DevS/Rv2027c 2-component signal transduction pathway to screen for novel antitubercular compounds. J. Biomol. Screen. *10*, 215–224.

Serafini, A., Pisu, D., Palù, G., Rodriguez, G.M., and Manganelli, R. (2013). The ESX-3 secretion system is necessary for iron and zinc homeostasis in *Mycobacterium tuberculosis*. PLoS ONE *8*, e78351.

Stoop, E.J., Bitter, W., and van der Sar, A.M. (2012). Tubercle bacilli rely on a type VII army for pathogenicity. Trends Microbiol. *20*, 477–484.

Takii, T., Yamamoto, Y., Chiba, T., Abe, C., Belisle, J.T., Brennan, P.J., and Onozaki, K. (2002). Simple fibroblast-based assay for screening of new antimicrobial drugs against *Mycobacterium tuberculosis*. Antimicrob. Agents Chemother. *46*, 2533–2539.

Zahrt, T.C., and Deretic, V. (2001). *Mycobacterium tuberculosis* signal transduction system required for persistent infections. Proc. Natl. Acad. Sci. USA *98*, 12706–12711.

Zahrt, T.C., Wozniak, C., Jones, D., and Trevett, A. (2003). Functional analysis of the *Mycobacterium tuberculosis* MprAB two-component signal transduction system. Infect. Immun. *71*, 6962–6970.